Effect of nanoscale curvature sign and bundle structure on supercritical H_2 and CH_4 adsorptivity of single wall carbon nanotube.

M. Yamamoto・T. Itoh・H. Sakamoto・T. Fujimori・K. Urita・Y. Hattori・T. Ohba・H. Kagita・H. Kanoh・S. Niimura・K. Hata・K. Takeuchi・M. Endo・F. Rodrígues-Reinoso・K. Kaneko

M. Yamamoto・T. Ohba・H. Kagita・H. Kanoh

Department of Chemistry, Graduate School of Science, Chiba University, 1-33 Yayoi, Inage, Chiba 263-8522, Japan

T. Itoh・H. Sakamoto・T. Fujimori・S. Niimura・K. Takeuchi・M. Endo・K. Kaneko (✉)

e-mail: kkaneko@shinshu-u.ac.jp

Research Center for Exotic Nanocarbons, Shinshu University, 4-17-1 Wakasato, Nagano, 380-8553, Japan

K. Urita

Department of Applied Chemistry, Nagasaki University, 1-14 Bunkyo, Nagasaki, 852-8521, Japan

Y. Hattori

Faculty of Textile Science and Technology, Shinshu University, 3-15-1 Tokida, Ueda-shi, 386-8567, Japan

K. Hata

National Institute of Advanced Industrial Science and Technology (AIST), Tsukuba, Ibaraki 305-8561, Japan

Japan Science and Technology Agency (JST), Kawaguchi 332-0012, Japan

F. Rodrígues-Reinoso

Departamento de Química Inorgánica, Universidad de Alicante, E-03080, Alicante, Spain

Instituto Universitario de Materiales de Alicante (IUMA), E-03080, Alicante, Spain

Abstract The adsorptivities of supercritical CH_4 and H_2 of the external and internal tube walls of single wall carbon nanotube (SWCNT) were determined. The internal tube wall of the negative curvature showed the higher adsorptivities for supercritical CH_4 and H_2 than the external tube wall of the positive curvature due to their interaction potential difference. Fine SWCNT bundles were prepared by the capillary force-aided drying treatment using toluene or methanol in order to produce the interstitial pore spaces having the strongest interaction potential for CH_4 or H_2; the bundled SWCNT showed the highest adsorptivity for supercritical CH_4 and H_2. It was clearly shown that these nanostructures of SWCNTs are crucial for supercritical gas adsorptivity.

Keywords *Carbon nanotube, Capillary force, Nanoscale curvature, Nanoporosity, Hydrogen adsorption, Methane adsorption*

1 Introduction

Single wall carbon nanotube consists of a rolled graphene (tube) and hemispherical caps at both ends (Iijima and Ichihashi 1993). Hence open single wall carbon nanotube has a cylindrical tube structure having external and internal tube walls of positive and negative nanoscale curvatures, respectively. The open single wall carbon nanotube has an extremely high geometrical surface area of 2630 m^2 g^{-1}, because all component carbon atoms are exposed to the external and internal walls. The sign of the nanoscale curvature should be essentially influential to adsorption properties for gases, because the interaction potential energies of a molecule with the single wall carbon nanotube wall of the different curvature sign are different each other. In particular, such a curvature sign difference should give an intensive effect on supercritical gas adsorption. This is because the molecule-single wall carbon nanotube interaction potential difference between the positive and negative curvatures is critical to adsorption under the supercritical conditions. Accordingly the relationship between the supercritical gas adsorptivity and the nanoscale curvature sign should be studied (Ohba et al. 2007). However, most single wall carbon nanotube have the bundle structure and thereby the dependence of the gas adsorption property on the curvature sign of the single wall carbon nanotube wall cannot be studied.

Hata et al. succeeded to prepare mutually isolated single wall carbon nanotubes (SWCNTs) of high purity using CVD method with isolated nanocatalyst particles embedded in the catalyst substrate; the SWCNT length is in an order of 1 mm (Hata et al. 2004). Hence, the tube opening of this type of SWCNTs enables to elucidate the relationship between the curvature sign difference and adsorptivity for supercritical gas.

It is well-known that interstitial pores in the bundled single wall carbon nanotube give the deepest interaction potential which favors for adsorption of supercritical gas. However, it is difficult to control the bundle structure for ordinary single wall carbon nanotube samples, because as-received single wall carbon nanotube sample has the bundled structure. As the major SWCNTs prepared by Hata et al. are isolated, we can control the bundle formation. SWCNTs well wet to an organic solvent and thereby simple drying of SWCNTs immersed in the organic solvent should produce a considerably firm bundle structure depending on the capillary force. Then we can also study the relationship between supercritical gas adsorptivity and bundle structure of SWCNT.

The global warming is a serious issue for the future of human being. We have a

great need for fundamental researches which are associated with clean energy storage. Supercritical H_2 and CH_4 are representatives of the clean fuels. In particular, supercritical H_2 doesn't emit any CO_2 on burning. Then H_2 is expected to be an ideally clean energy; the appropriate adsorbents for storage of H_2 have been actively studied (Assfour and Seifert 2010; Kim et al. 2007; Kockrick et al. 2010; Nishihara et al. 2009; Salvador et al. 2009; Tsao et al. 2010; Wenzel et al. 2009; Xua et al. 2007; Zheng et al. 2010). Although there are no greatly promising storage results for supercritical H_2 on SWCNTs, further understanding of physical adsorption mechanism of supercritical H_2 on well-designed SWCNTs systems is indispensable (Arai et al. 2009). CH_4 is the cleanest in the hydrocarbon fuels and then we should have a satisfied adsorbent for supercritical CH_4 (Kockrick et al. 2010; Menon and Komarneni 1998; Moellmer et al. 2010; Ottiger et al. 2008; Prauchner and Rodríguez-Reinoso 2008; Rejifu et al. 2009; Senkovska and Kaskel 2008; Solara et al. 2008; Urabe et al. 2008; Urbonaite et al. 2008). We must understand the relationship between nanostructure of adsorbents and CH_4 adsorptivity. Therefore, the adsorptivity of the nanostructure-controlled SWCNT for N_2 and CH_4 must be elucidated. This paper reports effect of the nanoscale curvature and bundle structure controlled by the capillary force-aided drying on adsorptivities of highly pure SWCNTs for supercritical H_2 and CH_4.

2 Experimental

The isolated SWCNTs were produced by the CVD method reported earlier (Hata et al. 2004). The SWCNTs were sonicated in toluene or methanol at 273 K for 12 h, and then they were aged for 24 h. After the treatment, they were filtrated and dried at 423 K in order to form the bundle structure using capillary force on the solvent evaporation. Thus-obtained SWCNT with toluene or methanol is denoted Tol-SWCNT or Met-SWCNT, respectively. The SWCNTs were also oxidized in a flow of N_2 and O_2 mixture (N_2:O_2 = 80:20) at the flow rate of 150 ml min^{-1} at 693 K for 1 h in order to remove caps selectively. This SWCNT sample is denoted Ox-SWCNT. The SWCNT samples were characterized with Raman spectroscopy (YAG laser: 532 nm, Ar laser: 633 nm, NRS-3100, JASCO), scanning electron microscopy (SEM) (JSM-6330F, JEOL), high resolution transmission electron microscopy (TEM) (JEM-4000FX, JEOL). The nanopore structure of the SWCNT samples was determined by N_2 adsorption at 77 K after pre-evacuation at 423 K and 10^{-4} Pa for 2 h with a volumetric apparatus (Quantachrome Co., Autosorb-MP-1); the pore structural parameters were

obtained by the subtracting pore effect (SPE) method (Gregg and Sing 1982; Kaneko et al. 1992) using the high resolution α_s-plot and DR analysis (Dubinin 1960). We measured high pressure adsorption isotherms of supercritical H_2 at 77 K and CH_4 at 303 K gravimetrically after the pre-evacuation at 423 K and 10^{-4} Pa for 2 h. The modified buoyancy-mediated method was used for evaluation of the adsorbed-layer volume, which is applied to the gravimetrically determined adsorption isotherm without the buoyancy correction (Noguchi et al. 2007).The particle densities of the SWCNT samples, which were indispensable to obtain the correct high pressure adsorption amounts, were measured with high pressure buoyancy method up to 6 MPa of He at 303 K after the pre-evacuation treatment same as the adsorption measurements (Kaneko et al. 1992).

3 Results and discussion

3.1 Nanopore structure control

Figure 1 shows N_2 adsorption isotherms of SWCNT samples at 77 K. The adsorption isotherms of SWCNT and Ox-SWCNT are close to IUPAC Type II, being the representative adsorption isotherm of a nonporous solid. However, both have a very sharp uptake near the ordinate; the real rising is observed around $P/P_0 = 10^{-3}$, as indicated in Fig.1 (b).

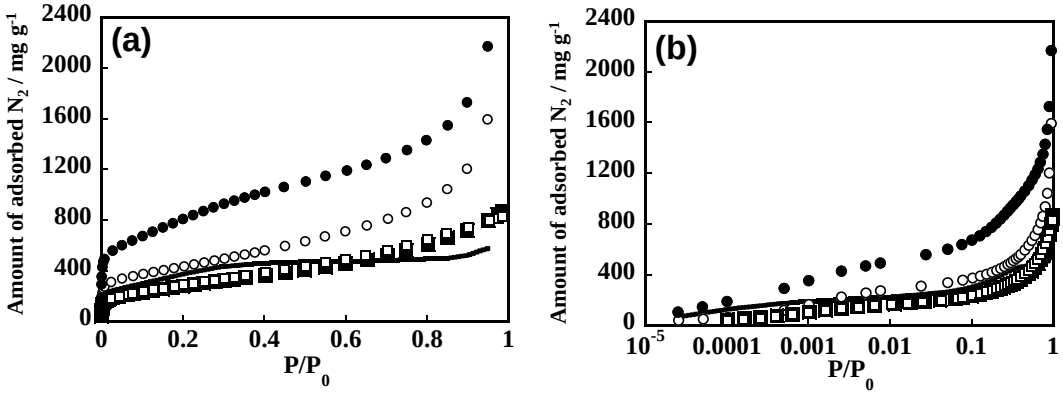

Fig. 1. Nitrogen adsorption isotherms at 77 K on the SWCNT samples. SWCNT(open circle), Ox-SWCNT(closed circle), Tol-SWCNT(open square), Met-SWCNT(closed square), and Int-SWCNT(solid line). The abscissa of the right figure (b) is expressed in terms of the logarithm of P/P_0.

The vertical uptake near the ordinate in Fig. 1 (a), being characteristic of IUPAC Type I, indicates the presence of nanopores where molecules are adsorbed with micropore filling mechanism. The Ox-SWCNT has much larger adsorption amount than SWCNT over the whole P/P_0 range, suggesting high accessibility of

N_2 molecules to the internal tube spaces. We evaluated the adsorption isotherm of internal tube spaces of SWCNT by subtracting adsorption isotherm of SWCNT from that of Ox-SWCNT, being denoted Int-SWCNT. The N_2 adsorption isotherm of Int-SWCNT is of almost equivalent of Type I, agreeing with the presence of the internal tube spaces in a nm scale. On the other hand, the adsorption amounts of Tol- and Met-SWCNTs are much smaller than that of untreated SWCNT. The adsorption isotherms of both samples are rather close to the IUPAC Type I, indicating that those samples are nanoporous and adsorption on the external surface is not predominant. These N_2 adsorption isotherms were analyzed by the SPE and DR methods, providing the nanopore structural parameters, as shown in Table 1.

Table 1. Surface area and nanopore volume evaluated by SPE and DR methods

	Surface area / $m^2\ g^{-1}$	**Nanopore volume / $cm^3\ g^{-1}$**
SWCNT	**1040**	**—**
Ox-SWCNT	**1900**	**0.80**
Tol-SWCNT	**590**	**0.27**
Met-SWCNT	**600**	**0.27**

The surface area of Ox-SWCNT is 1900 $m^2\ g^{-1}$, being the most close to the surface area of graphene (2630 $m^2\ g^{-1}$), being about twice of that of SWCNT. The nanopore volume of Ox-SWCNT is 0.80 $cm^3\ g^{-1}$ and thereby the average tube diameter is estimated to be 2.5 nm under the assumption of absence of the bundle structure. TEM observations of SWCNT gave 3.0 nm of the mean diameter between the carbon atom centers on the wall (Futaba et al. 2006). Hence, our estimated average tube diameter of 2.5 nm from N_2 adsorption is reasonable, because the effective tube space diameter can be approximated by the difference between 3.0 nm and 0.34 nm of the graphene thickness.

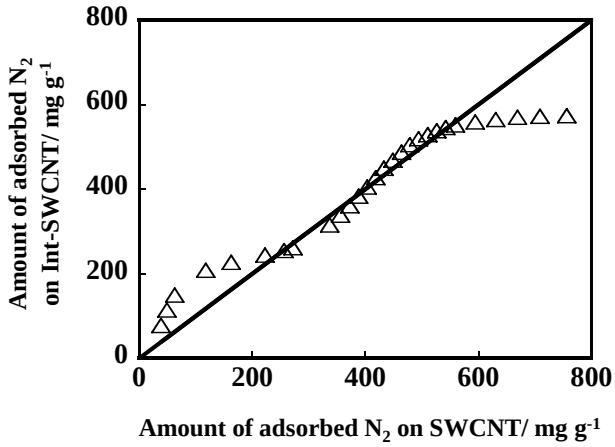

Fig. 2. Comparison plot of nitrogen adsorption isotherm of Int-SWCNT against that of SWCNT. The amount of adsorbed nitrogen on Int-SWCNT was normalized by the surface area ratio of Int-SWCNT over SWCNT. The solid line shows that adsorption amounts of both samples are equal to each other.

Comparison plot of normalized Int-SWCNT against SWCNT is shown in Fig. 2. The amount adsorbed N_2 on Int-SWCNT in Fig. 2 should be normalized, the external and internal wall surfaces have different surface areas and thereby the adsorptivity must be compared using the adsorption amount per the effective surface area. The normalization coefficient of 1.2 was determined using the observed surface areas of SWCNT and Ox-SWCNT. The upward deviation in the smaller adsorption range indicates the presence of stronger monolayer adsorption sites in Int-SWCNT (monolayer capacity = 300 mg g^{-1}) than in SWCNT. Therefore, it is possible to infer that the internal tube wall of a negative curvature of Int-SWCNT has a stronger surface-molecule interaction than the external tube wall of a positive curvature of SWCNT. The comparison plot almost overlaps with the solid line after the accomplishment of monolayer adsorption, because the curvature sign difference does not markedly influence the adsorption on the monolayers on the internal and external pore walls. Then, the comparison plot is downward deviated becoming parallel to the abscissa owing to the adsorption limitation in the nanopores.

Table 1 also shows Tol- and Met-SWCNT samples have the smallest SPE surface areas of 590 and 600 $m^2 g^{-1}$, respectively, indicating the decrease in the external surface area of SWCNTs due to the formation of the bundle structures. This surface area value suggests the presence of the fine bundle of three to four SWCNTs whose average diameter is about 5 nm. Consequently, the drying after simple sonication treatment with toluene or methanol induces the fine bundle

formation. Although interstitial pores are produced by the bundle formation, N_2 molecules cannot be adsorbed in those spaces due to their narrow diameters.

Figure 3 shows SEM images of SWCNT and treated SWCNT samples. The SEM image of Ox-SWCNT is almost similar to that of SWCNT. Tol-SWCNT and Met-SWCNT have a continuous structure, suggesting the bundle and entangled assembly formation. This indicates that capillary drying-treatment using toluene or methanol brings about a unique associated structure of SWCNTs. The assembly structures of both treated SWCNT samples are different from each other. TEM images of SWCNT samples are shown in Fig. 4.

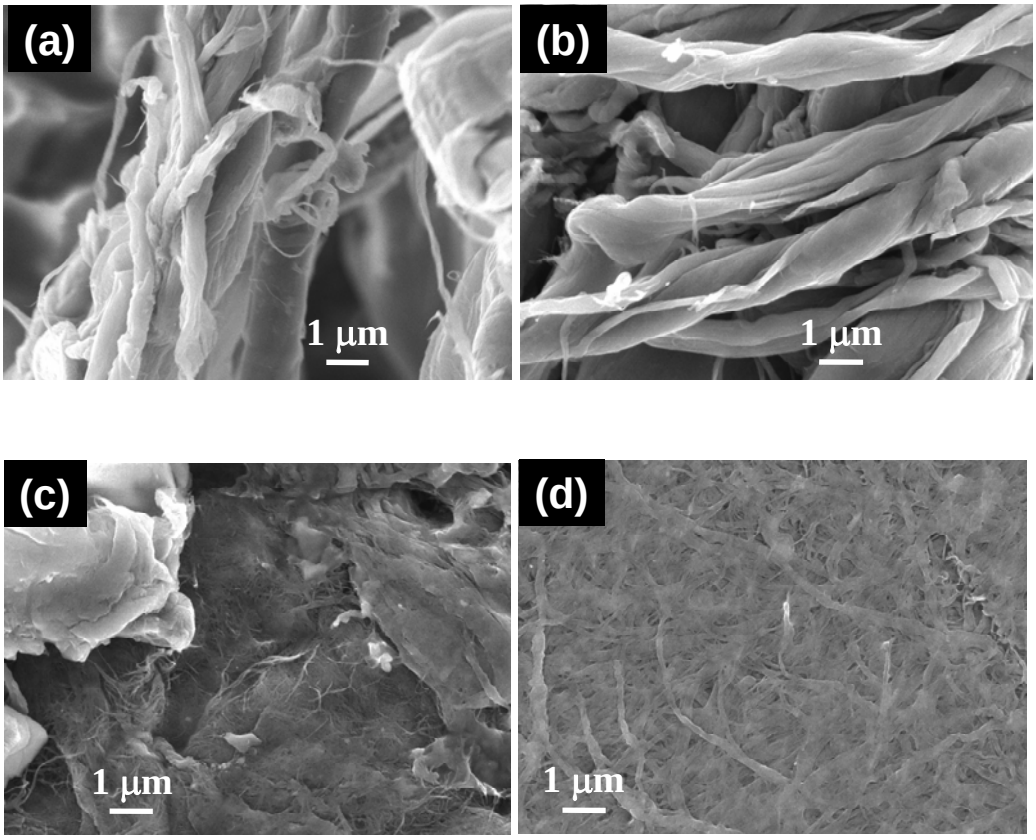

Fig. 3. SEM images of the SWCNT samples, (a) SWCNT, (b) Ox-SWCNT, (c) Tol-SWCNT, and (d) Met-SWCNT.

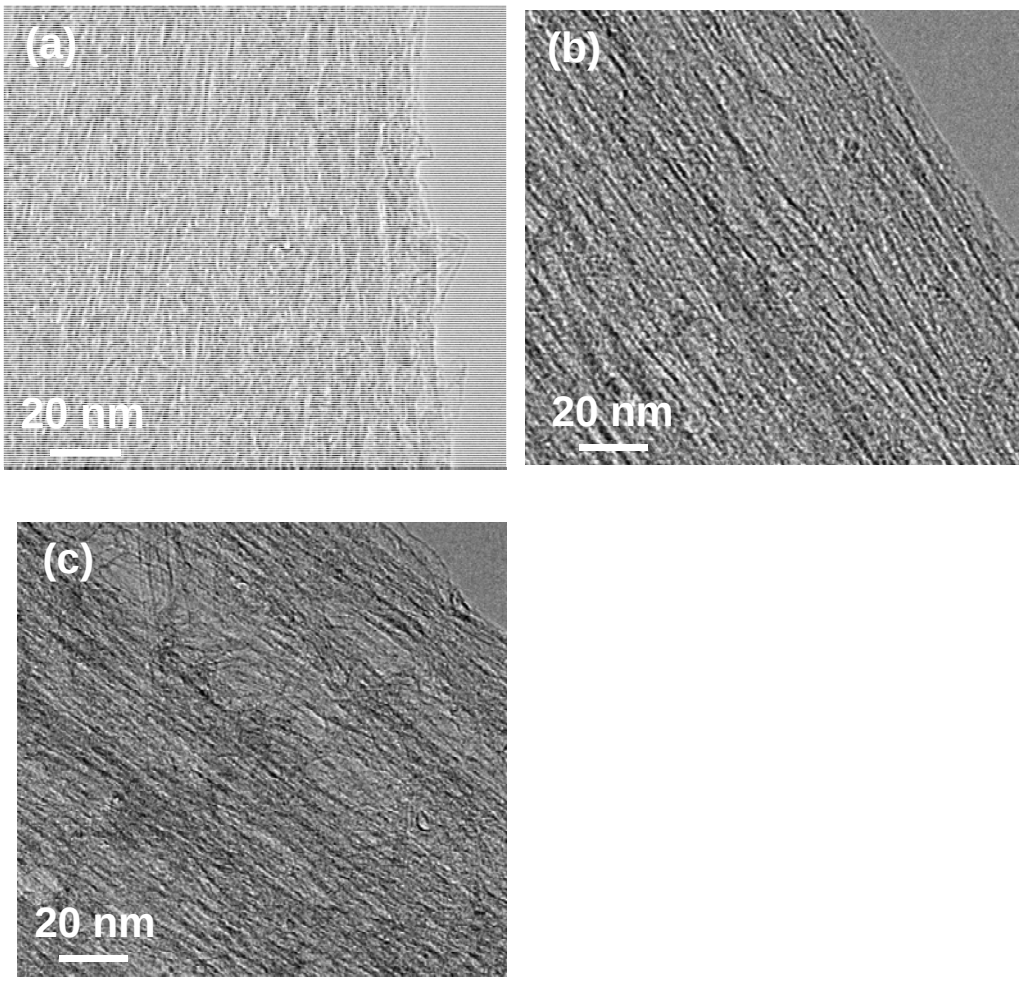

Fig. 4. TEM images of the SWCNT samples, (a) SWCNT, (b) Tol-SWCNT, and (c) Met-SWCNT

All images are close to each other. However, we can observe well-oriented bundle structures in the TEM images of Tol-SWCNT and Met-SWCNT; Tol-SWCNT has better oriented structure. Then, the capillary force-aided treated SWCNT has a fine bundle structure. However we cannot evaluate the average bundle size from the TEM image, although the above-mentioned N_2 adsorption analysis can give an estimated value of the bundle size.

Removal of caps from SWCNT by oxidation can be also evidenced by the particle density data from the high pressure buoyancy plot. Figure 5 shows He buoyancy plots of SWCNT samples. All plots are linear except for an upward deviation near the ordinate. The initial upward deviation comes from adsorption of He in very narrow nanopores. The contribution by He adsorption can be precisely corrected by the extrapolation of the linear relationship in the high pressure range of He.

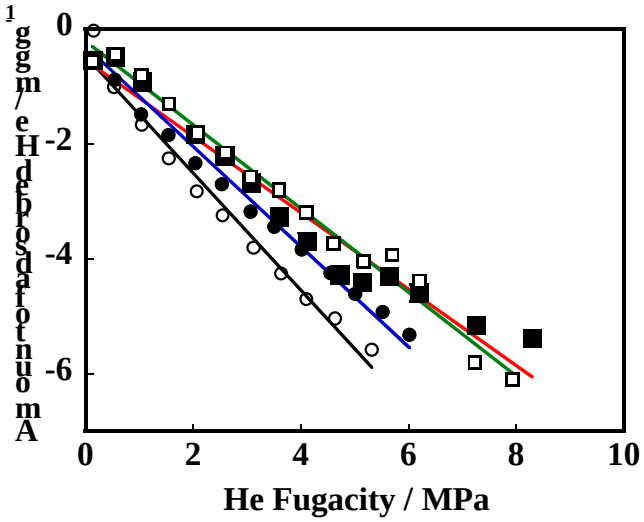

Fig. 5. He buoyancy curves at 303 K. SWCNT(open circle), Ox-SWCNT(closed circle), Tol-SWCNT(open square), and Met-SWCNT(closed square).

The particle densities of SWCNT samples determined from the slope of the linear relationship are listed in Table 2. The particle density of Ox-SWCNT is close to the solid density of graphite (2.27 g cm^{-3}), whereas the particle densities of Tol- and Met-SWCNT samples are much less than the solid density of graphite. Consequently, Ox-SWCNT has almost a perfectly open tube structure of graphene of positive and negative curvatures.

Table 2. Particle density of the SWCNT samples]

	Particle density / g cm^{-3}
SWCNT	**1.56**
Ox-SWCNT	**2.13**
Tol-SWCNT	**1.58**
Met-SWCNT	**1.60**

If we assume that the density of the wall of the SWCNT is equal to that of graphite, an opening ratio r_{op} of Ox-SWCNT, is obtained from the following relationship.

$$r_{op} = \frac{\rho_s - \rho_0}{\rho_g - \rho_0} \qquad (1)$$

Here, ρ_s, ρ_g, and ρ_0 are the densities of the treated SWCNT sample, graphite, and untreated SWCNT, respectively. Here, the opening ratio denotes the availability

of the internal tube spaces for adsorption. The r_{op} of Ox-SWCNT is 0.80. The density of the carbon wall should be smaller than that of a perfect graphite due to the presence of various defects; therefore, the r_{op} of Ox-SWCNT should be larger than 0.80.

We can determine the SWCNT tube diameter distribution from the radial breathing mode (RBM) of the Raman bands (Jorio et al. 2003). Figure 6 shows the RBM bands of the SWCNT samples in the wave number range of 100 to 300 cm^{-1} at room temperature. There are several RBM peaks of SWCNT, which indicate the presence of distribution of the tube diameter from 0.83 nm to 1.4 nm (Araujo et al. 2008). The RBM bands do not change on the oxidation and the capillary force-aided drying treatments. These treatments do not change the SWCNT structure itself.

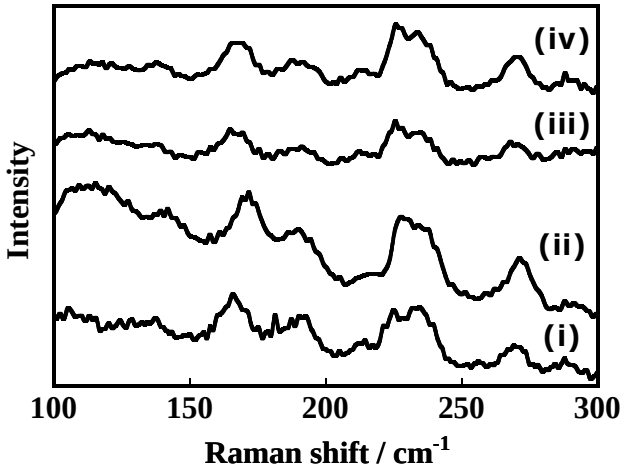

Fig. 6. RBM Raman bands of the SWCNT samples, (i) SWCNT, (ii) Ox-SWCNT, (iii) Tol-SWCNT, and (iv) Met-SWCNT.

3.2 Graphitic structures

Raman spectrum of SWCNT has both of G and D bands at 1594 cm^{-1} and 1330 cm^{-1}, respectively, which can be used for evaluation of graphitic crystallinity. Although SWCNT is highly pure, the D band is considerably strong and thereby the crystallinity is not so good, suggested by the TEM observation. The capillary force-aided drying treatment or oxidation process increases the G/D band ratio (2.6 for SWCNT, 3.8 for Tol-SWCNT, 4.0 for Met-SWCNT, and 6.6 for Ox-SWCNT). Accordingly, the treatment should remove amorphous structural parts from the SWCNT.

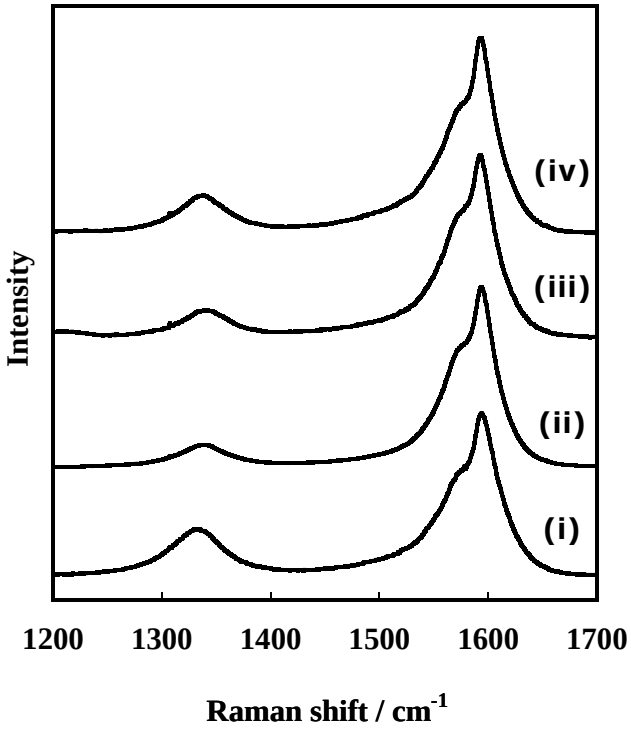

Fig. 7. Raman spectra of the SWCNH samples from 1200 to 1700 cm^{-1}, (i) SWCNT, (ii) Ox-SWCNT, (iii) Tol-SWCNT, and (iv) Met-SWCNT.

3.3 Adsorptivities of SWCNT for supercritical H_2 and CH_4.

Figure 8 shows adsorption isotherms of H_2 on SWCNT samples up to 101 kPa and 7 MPa at 77 K.

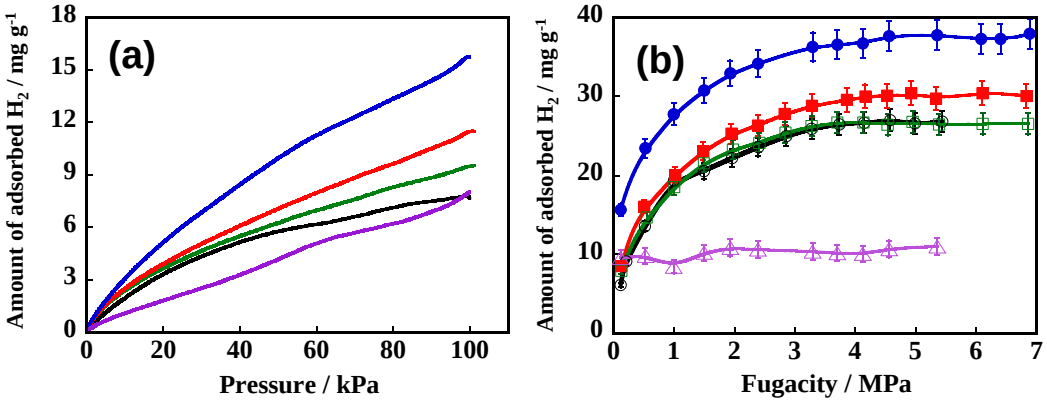

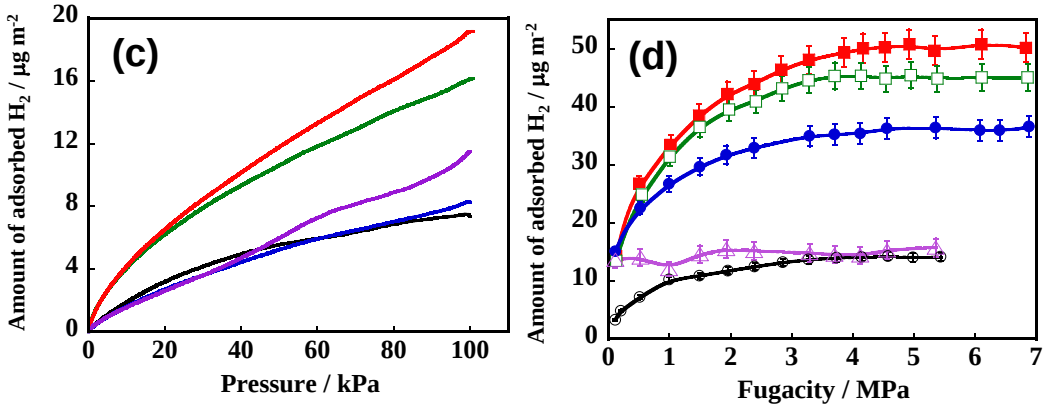

Fig. 8. H_2 adsorption isotherms at 77 K on the SWCNT samples. SWCNT(black), Ox-SWCNT(blue), Tol-SWCNT(green), Met-SWCNT(red), and Int-SWCNT(purple). Up to (a), (c) 101 kPa and (b), (d) 7 MPa. The ordinate of figures (c) and (d) are expressed by unit per surface area of the samples. The adsorption amount isotherm of Int-SWCNT was corrected by experimental surface difference between the external and internal tube walls in figures (c) and (d).

The adsorption amount in Fig. 8 (a) and (b) is expressed by mg per unit weight SWCNT sample. Ox-SWCNT has the greatest adsorption amount due to the largest surface area. However, both of the capillary-force aided drying treated SWCNTs have slightly larger adsorption amounts than untreated SWCNT irrespective of the half of the surface area. Quite important features are obtained from Fig. 8 (c) and (d) of which ordinates are expressed by H_2 adsorbed amount per effective unit surface area. In this case both of bundled SWCNT samples have the greatest adsorption amount, indicating that supercritical H_2 is adsorbed in the interstitial sites of the strongest interaction potential. Probably Tol-SWCNT has a more firmly associated structure than Met-SWCNT, as indicated by the TEM observation. Adsorption amount of Int-SWCNT is larger than that of untreated SWCNT above about 40 kPa, although both H_2 adsorption amounts are much smaller than the bundled SWCNT samples in the lower pressure region. The important point is that the adsorption sites of negative curvature are more effective than that of positive curvature.

The remarkable effect of the capillary force-aided drying treatment is also observed in high pressure CH_4 adsorption, as shown in Fig. 9. Figure 9(a) shows the high pressure CH_4 adsorption isotherms at 303 K in terms of mg per g-adsorbent. The order of the high pressure adsorption amount is Ox-SWCNT, the treated SWCNT, and SWCNT. The adsorption amount of the treated SWCNT is

1.7 times larger than that of SWCNT, although their nanopore volume is a half of SWCNT.

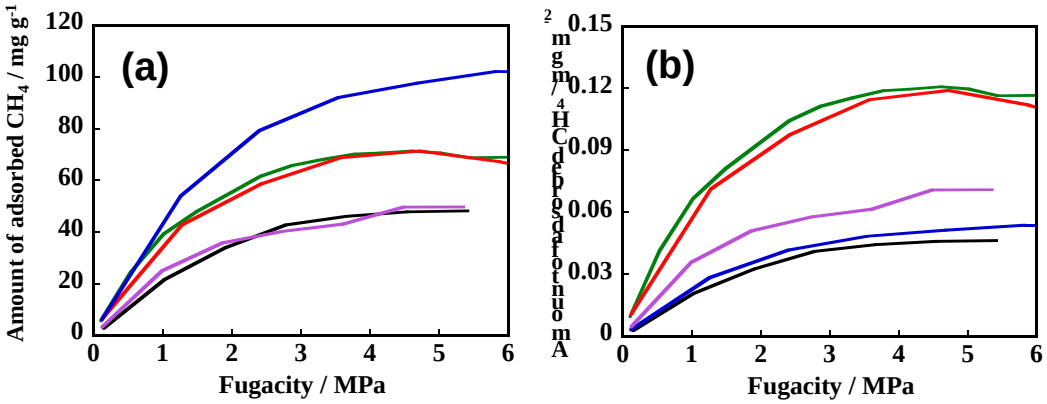

Fig. 9. Methane adsorption isotherms at 303 K per unit weight (a) and unit surface area (b) of the SWCNT samples, SWCNT(black), Ox-SWCNT(blue), Tol-SWCNT(green), Met-SWCNT(red), and Int-SWCNT(purple). The adsorption amount in Fig. 9 (b) is corrected taking into account the geometrical surface area difference between the external and internal tube walls.

The efficient adsorptivity for CH_4 can be understood from CH_4 adsorption isotherm in terms of mg per unit surface area, as shown in Fig. 9 (b). The greatest adsorptivities of Tol-SWCNT and Met-SWCNT for CH_4 are really noteworthy, being nearly three-times larger than those of SWCNT and Ox-SWCNT. Also this figure clearly shows that the concave wall of the negative curvature is more effective for adsorption of supercritical CH_4 than the convex wall of the positive curvature. As supercritical CH_4 adsorption needs enough strong adsorption sites, the strength difference of the adsorption sites can be explicitly shown as Fig. 9. (b). A similar result for efficient adsorptivities for H_2 was also shown, although the effect was less marked.

3.4 Nanoscale Curvature Sign Dependence of Interaction Potential and Interstitial Pore Structure

This experimental study shows explicitly that the adsorptivities for CH_4 and H_2 depends on the sign of the tube curvature of SWCNT. Figure 10 shows the interaction potential profiles of SWCNT with CH_4 and H_2 using molecule-nanopore interaction potential using the established potential functions for carbon cylinder of an infinite length. (Tjatjopoulos et al. 1988; Murata et al. 2001). The interaction potential depth for the internal wall of the negative curvature is

much deeper than that for the external wall of the positive curvature for CH_4 and H_2. CH_4 gives a larger difference than H_2. Thus adsorptivity of SWCNT for a supercritical gas showed sensitively depends on the sign of the tube curvature, as observed in this study. As the interaction between the SWCNT and gas is not enough to induce a predominant adsorption, the potential difference interaction between the internal and external tube walls can be detected by supercritical gas adsorptivity.

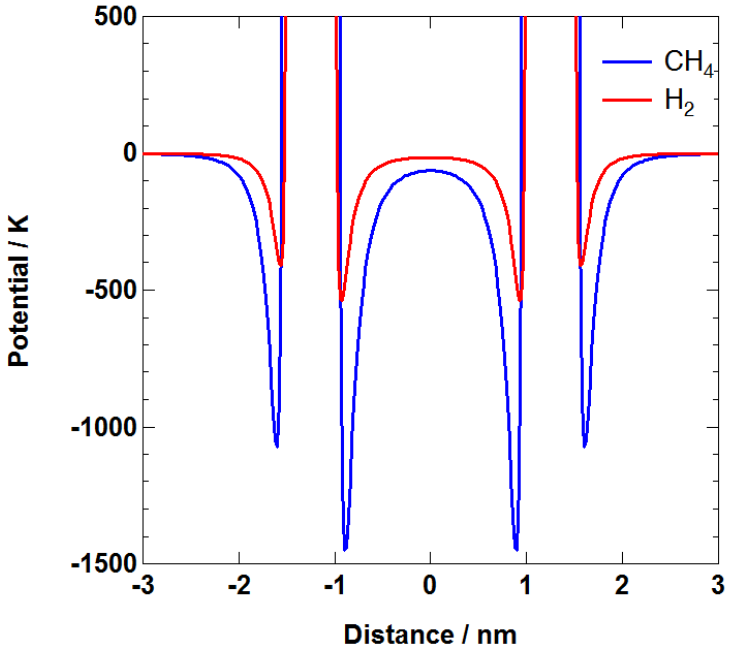

Fig. 10. Potential profiles of H_2 and CH_4 adsorbed on the internal and external 2.5 nm-diameter SWCNT. Lennard-Jones parameters are as follows. CH_4; σ_{ff} = 0.3721 nm and ε_{ff}/k_B = 161.3 K, H_2; σ_{ff} = 0.2958 nm and ε_{ff}/k_B = 36.7 K, and carbon atom in the SWCNT; σ_{ss} = 0.34 nm and ε_{ss}/k_B = 28.0 K.

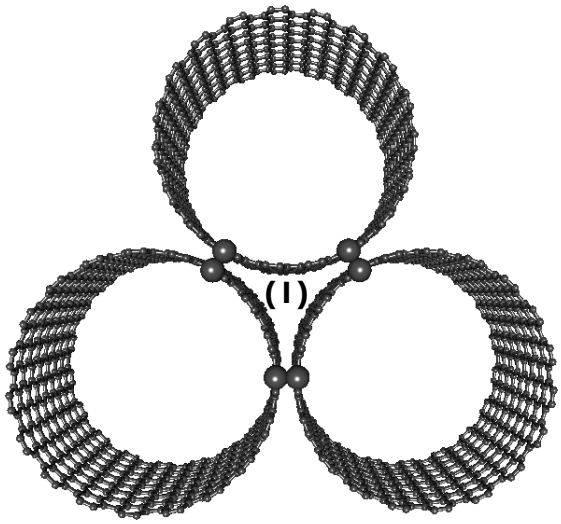

Fig. 11. Homo-tube SWCNT bundle model of the triangular geometry. (I): Interstitial pore space. Here a realistic tube-tube contact is expressed only by the contact point in order to express the carbon hexagon-network structure.

In case of the bundled SWCNTs, as shown in Fig. 11, the interstitial pore space surrounded by three convex walls has the deepest interaction potentials of -3241 K for CH_4 and -1043 K for H_2. These potential depths for CH_4 and H_2 are deeper than those of the internal wall by 1789 K and 507 K, respectively. These potential energy differences are much larger than the thermal energy at the measuring temperature (303 K for CH_4 and 77 K for H_2). Accordingly these interstitial pore spaces are the most efficient for adsorption of supercritical CH_4 and H_2. Here we need to consider the reduction of N_2 adsorption by the bundle formation. The Lennard-Jones size parameter of N_2 is 0.3632 nm, being smaller than that of CH_4. If CH_4 molecules are adsorbed in the interstitial pore spaces, the N_2 molecules must be adsorbed in the sites. However, N_2 adsorption was measured at the boiling point of liquid N_2 and thereby the N_2 molecules are adsorbed at the entrance ports of the interstitial pore spaces very strongly, blocking the further adsorption. On the other hand, N_2 molecules are adsorbed even on the external pore walls sufficiently at 77 K. Accordingly, the effective surface area evaluated by N_2 adsorption for the capillary force-aided drying treated SWCNT samples is much smaller than that of the untreated SWCNT.

In the above discussion, we just used the simple SWCNT model of the average tube diameter. However, the Raman examination indicates the distribution of the tube diameter of SWCNT from 0.83 nm to 1.4 nm. Also, the preceding TEM observation (Futaba et al. 2006) showed the tube diameter distribution from 1 to 5 nm. Consequently, the real SWCNT bundles should contain hetero-tube bundles of which diameters are different from each other. The possible size of the interstitial pore spaces for the homo-tube bundles of the triangular geometry is in the range of 0.21 nm to 0.83 nm. The estimated interstitial pore size of the hetero-tube bundles is included in this range. Also the average size of the possible size range is 0.52 nm, which is reasonable for above discussion. Supercritical CH_4 and H_2 are tightly adsorbed, whereas a serious entrance blocking occurs for N_2 adsorption at 77 K.

4 Conclusion

As the interaction of single wall carbon nanotube (SWCNT) with supercritical

H_2 and CH_4 is not sufficiently strong, it is clearly shown that the internal tube walls of SWCNT having the negative curvature has higher adsorptivity for supercritical H_2 and CH_4 than the external tube walls having the positive curvature. The adsorption study using SWCNT bundles prepared from isolated SWCNTs explicitly evidenced the important contribution of the interstitial pores in adsorption for supercritical H_2 and CH_4.

Acknowledgements This work was supported by Japan Science and Technology Agency Strategic Japanese-Spanish Cooperative Program: Nanotechnologies and New Materials for Environmental Challenges and Grant-in-Aid for Scientific Research (A) (No. 21241026). K. Kaneko, T. Itoh, and T. Fujimori were supported by Exotic Nanocarbons, Japan Regional Innovation Strategy Program by the Excellence, Japan Science and Technology Agency.

References

Assfour B., Seifert G.: Adsorption of hydrogen in covalent organic frameworks: Comparison of simulations and experiments. Micropor. Mesopor. Mater. **133**, 59-65 (2010)

Arai M., Utsumi S., Kanamaru, M., Urita, K., Fujimori, T., Yoshizawa N., Noguchi D., Nishiyama K., Hattori Y., Okino F., Ohba, T., Tanaka H., Kanoh, H., Kaneko K.: Enhanced hydrogen adsorptivity of single-wall carbon nanotube bundles by one-step C60-pillaring method. Nano Lett. **9**, 3694-3698 (2009)

Araujo P.t., Maciel I.O., Pesce P.B.C. Pimenta M.A., Doorn S.K., Qian H., Hartschuh A., Steiner M.,Grigorian L., Hata K., Jorio A.: Nature of the constant factor in the relation between radial breathing mode frequency and tube diameter for single-wall carbon nanotubes. Phys. Rev. B **77**, 241403 (2008)

Dubinin M.M.: The potential theory of adsorption of gases and vapors for adsorbents with energetically nonuniform surfaces. Chem. Rev. **60**, 235-241 (1960)

Futaba D.N., Hata K.,Namai T., Yamada T., Mizuno K., Hayamizu Y., Yumura M., Iijima S.: 84% catalyst activity of water-assisted growth of single walled carbon nanotube forest characterization by a statistical and macroscopic approach. J. Phys. Chem. B **110**, 8035-8038 (2006)

Gregg, S.J., Sing, K.S.W.: Adsorption, Surface Area and Porosity. Academic Press, New York (1982). pp. 41

Hata K., Futaba D.N., Mizuno K., Namai T., Yumura M., Iijima S.: Water-assisted highly efficient synthesis of impurity-free single-walled carbon nanotubes. Science **306**, 1362-1364 (2004)

Iijima S., Ichihashi T.: Single-shell carbon nanotubes of 1-nm diameter. Nature **363**, 603-605 (1993)

Jorio, A., Pimenta, M.A., Filho, A.G.S., Saito, R., Dresselhaus, G., Dresselhaus, M.S.: Characterizing carbon nanotube samples with resonance Raman scattering. New J. Phys. **5** 139.1-139.17 (2003)

Kaneko, K., Ishii, C., Ruike, M., Kuwabara, H.: Origin of superhigh surface area and microcrystalline graphitic structures of activated carbons. Carbon **30**, 1075-1088 (1992)

Kaneko K., Shimizu K., Suzuki T.: lntrapore field-dependent micropore filling of supercritical N_2 in slit-shaped micropores. J. Chem. Phys. **97**, 8705-8711 (1992)

Kim D.-Y., Yang C.-M., Yamamoto M., Lee D.-H., Hattori Y., Takahashi K., Kanoh H., Kaneko K.: Supercritical hydrogen adsorption of ultramicropore-enriched single-wall carbon nanotube sheet. J. Phys. Chem. C **111**, 17448-17450 (2007)

Kockrick E., Schrage C., Borchardt L., Klein N.: Rose M., Senkovska I., Kaskel S.: Ordered mesoporous carbide derived carbons for high pressure gas storage. Carbon **48**, 1707-1717 (2010)

Menon V.C., Komarneni S.: Porous Adsorbents for Vehicular Natural Gas Storage: A Review. J. Porous Mater. **5**, 43-58 (1998)

Moellmer J., Celer E.B., Luebke R., Cairns A.J., Staudt R., Eddaoudi M., Thommes M.: Insights on adsorption characterization of metal-organic frameworks: A benchmark study on the novel soc-MOF. Micropor. Mesopor. Mater. **129**, 345-353 (2010)

Murata K., Kaneko K., Steele W.A., Kokai F., Takahashi K., Kasuya D., Hirahara K., Yudasaka M., Iijima S.: Molecular potential structures of heat-treated single-wall carbon nanohorn assemblies. J.

Phys. Chem. B 105, 10210-10216 (2001)
Nishihara H., Hou P.-X., Li L.-X., Ito M., Uchiyama M., Kaburagi T., Ikura A., Katamura J., Kawarada T., Mizuuchi K., Kyotani T.: High-pressure hydrogen storage in zeolite-templated carbon. J. Phys. Chem. C **113**, 3189–3196 (2009)
Noguchi H., Kondo A., Hattori Y., Kajiro H., Kanoh H., Kaneko K.: Evaluation of an Effective Gas Storage Amount of Latent Nanoporous Cu-Based Metal-Organic Framework. J. Phys. Chem. C **111**, 248-254 (2007)
Ohba T., Matsumura T., Hata K., Yumura M., Iijima S., Kanoh H., Kaneko K.: Nanoscale curvature effect on ordering of N2 molecules adsorbed on single wall carbon nanotube. J. Phys. Chem. C **111**, 15660-15663 (2007)
Ottiger S., Pini R., Storti G., Mazzotti M.: Competitive adsorption equilibria of CO_2 and CH_4 on a dry coal. Adsorption **14**, 539-556 (2008)
Prauchner M.J., Rodríguez-Reinoso F.: Preparation of granular activated carbons for adsorption of natural gas. Micropor. Mesopor. Mater. **109**, 581–584 (2008)
Rejifu A., Noguchi H., Ohba T., Kanoh H., Rodríguez-Reinoso F., Kaneko K.: Adsorptivities of Extremely High Surface Area Activated Carbon Fibres for CH_4 and H_2. Adsorp. Sci. Tech. **27**, 877-882 (2009)
Salvador F., Sánchez-Montero M.J., Montero, J., Izquierdo C.: Hydrogen storage in carbon fibers activated with supercritical CO_2: Models and the importance of porosity. J. Power Sources **190**, 331-335 (2009)
Senkovska I., Kaskel S.: High pressure methane adsorption in the metal-organic frameworks $Cu_3(btc)_2$, $Zn_2(bdc)_2dabco$, and $Cr_3F(H_2O)_2O(bdc)_3$. Micropor. Mesopor. Mater. **112**, 108-115 (2008)
Solara C., Sardellab F., Deianab C., Lagoc R.M., Vallonea A., Sapaga K.: Natural gas storage in microporous carbon obtained from waste of the olive oil production. Mater. Research **11**, 409-414 (2008)
Tjatjopoulos G.J., Feke D.L., Mann J.A.Jr.: Molecule-micropore interaction potentials. J. Phys. Chem. **92**, 4006-4007 (1988)
Tsao C.-S., Tzeng Y.-R., Yu M.-S., Wang C.-Y., Tseng H.-H., Chung T.-Y., Wu H.-C., Yamamoto T., Kaneko K., Chen S.-H.: Effect of catalyst size on hydrogen storage capacity of Pt-impregnated active carbon via spillover. J. Phys. Chem. Lett. **1**, 1060-1063 (2010)
Urabe Y., Ishikura T., Kaneko K.: Development of porosity in carbons from yeast grains by activation with alkali metal carbonates. J. Colloid Interf. Sci. **319**, 381-383 (2008)
Urbonaite S., Juárez-Galán J.M., Leis J. Rodríguez-Reinoso F., Svensson G.: Porosity development along the synthesis of carbons from metal carbides. Micropor. Mesopor. Mater. **113**, 14–21 (2008)
Wenzel S.E., Fischer M., Hoffmann, F., Fröba M.: Highly porous metal-organic framework containing a novel organosilicon linker - A promising material for hydrogen storage. Inorg. Chem. **48**, 6559-6565 (2009)
Xua W.-C., Takahashi K., Matsuo Y., Hattori Y., Kumagai M., Ishiyama S., Kaneko K., Iijima S.: Investigation of hydrogen storage capacity of various carbon materials. Int. J. Hydrogen Energy **32**, 2504-2512 (2007)
Zheng Z., Gao Q., Jiang J.: High hydrogen uptake capacity of mesoporous nitrogen-doped carbons activated using potassium hydroxide. Carbon **48**, 2968-2973 (2010)